# Climate models with delay differential equations

Andrew Keane,[a] Bernd Krauskopf,[b] and Claire M. Postlethwaite[c]
*University of Auckland, Auckland, New Zealand*

(Received 15 May 2017; accepted 14 August 2017; published online 17 October 2017)

A fundamental challenge in mathematical modelling is to find a model that embodies the essential underlying physics of a system, while at the same time being simple enough to allow for mathematical analysis. Delay differential equations (DDEs) can often assist in this goal because, in some cases, only the delayed effects of complex processes need to be described and not the processes themselves. This is true for some climate systems, whose dynamics are driven in part by delayed feedback loops associated with transport times of mass or energy from one location of the globe to another. The infinite-dimensional nature of DDEs allows them to be sufficiently complex to reproduce realistic dynamics accurately with a small number of variables and parameters. In this paper, we review how DDEs have been used to model climate systems at a conceptual level. Most studies of DDE climate models have focused on gaining insights into either the global energy balance or the fundamental workings of the El Niño Southern Oscillation (ENSO) system. For example, studies of DDEs have led to proposed mechanisms for the interannual oscillations in sea-surface temperature that is characteristic of ENSO, the irregular behaviour that makes ENSO difficult to forecast and the tendency of El Niño events to occur near Christmas. We also discuss the tools used to analyse such DDE models. In particular, the recent development of continuation software for DDEs makes it possible to explore large regions of parameter space in an efficient manner in order to provide a "global picture" of the possible dynamics. We also point out some directions for future research, including the incorporation of non-constant delays, which we believe could improve the descriptive power of DDE climate models. *Published by AIP Publishing.*
https://doi.org/10.1063/1.5006923

**In many climate systems, processes interact to form positive (destabilising) or negative (stabilising) feedback loops, which play pivotal roles for the stability and sensitivity of climate phenomena. Such feedback mechanisms are generally associated with delays due to transportation times of mass or energy over large distances. The relevant delay times depend on the climate system studied and may differ vastly across a large range of time scales, depending on intermediate processes involved in the respective feedback loops. To derive a conceptual climate model that is amenable to mathematical study, one approach has been to incorporate delayed feedback terms explicitly and obtain a delay differential equation (DDE). This paper offers a brief review of how DDEs have been introduced as conceptual climate models in different contexts, and what they are able to say about the dynamics and stability of the climate systems under consideration. The emphasis is on more recent results that have utilised advanced numerical methods for the bifurcation analysis of DDEs.**

## I. INTRODUCTION

Climate models can take many different forms. On the one hand, there exist sophisticated forecasting models derived from first principles known as General Circulation Models (GCMs). GCMs are very complex, often with millions of variables and parameters, and require vast amounts of time and computational resources to simulate. The use of GCMs for making climate predictions is currently common practice; however, they may suffer from a large number of parameter uncertainties and can potentially contain large errors; for example, see Ref. 9 and references therein. On the other hand, conceptual climate models are designed to investigate the interactions of key mechanisms in a climate system, such that their governing equations are much simpler and can be analysed mathematically. Therefore, conceptual climate models have proven very useful for investigating the fundamental properties of a climate system. Generally, conceptual models are developed in order to describe empirical relationships observed in nature. In some cases, they can also be derived from more complex models (that is, more "realistic" models) by making suitable physical assumptions or approximations; for example, see Refs. 25 and 51. Conceptual climate models have even been used to make predictions; for example, to provide an insight into sea-level rise response to emissions[81] and to predict how stable a climate system is against global climate change.[113]

Common components of conceptual climate models are positive or negative feedback mechanisms, which amplify or diminish, respectively, any changes in system variables. Understanding how different types of feedback affects the dynamics of a system, and how multiple feedback mechanisms interact with one another, is therefore of vital importance for understanding the observed behaviour of a climate

[a]a.keane@auckland.ac.nz
[b]b.krauskopf@auckland.ac.nz
[c]c.postlethwaite@auckland.ac.nz

system. Feedback loops occur naturally in climate systems on a variety of time scales, mainly as a result of mass or energy transport across the globe and/or throughout the atmosphere. Consider, for example, energy-balance models (EBMs), which focus on the global balance between incoming and outgoing radiation on the Earth. In the palaeoclimate context of investigating transitions between glacial and interglacial states, the time scales of interest are $10^3$–$10^5$ years.[5] There exists a fundamental feedback loop in EBMs because the global temperature of the Earth depends on the albedo of the Earth, which measures how much incoming solar radiation is reflected back into space. In turn, the albedo is related to the level of snow/ice cover, which depends on the global temperature. Yet, it can take a long time for ice of a significant size on the global scale to form or melt. Therefore, albedo values do not depend on present temperatures alone, but on temperatures in the past; in other words, there is a reaction delay in the system on the order of $10^3$–$10^4$ years.

Another important example, where feedback mechanisms play a role in climate variability, is the El Niño Southern Oscillation (ENSO) system, which is a coupled climate system with an oceanic component (El Niño) and an atmospheric component (Southern Oscillation). Figure 1 provides evidence for this coupling. The blue curve in panel (a) displays the average anomaly in the sea-surface temperature (SST) in the eastern Pacific Ocean (NINO3 index) and the red curve is the normalised surface air pressure difference between Tahiti and Darwin, Australia (Southern Oscillation Index; SOI), throughout the years 1964–2014. Generally, the blue and red time series are in anti-phase synchronisation, so that high NINO3 indices coincide with low SOI and vice-versa. There are many extrema in both time series of Fig. 1(a) on a small, intra-seasonal time-scale. However, it is only the larger peaks in the NINO3 index that represent the El Niño events, the warm phase of ENSO, while large drops represent the cool phase known as La Niña. These events tend to occur every four to seven years with significant variability in strength. Interdecadal variability can also be seen in panel (a). What is not so clear in the time series, yet is commonly known, is that El Niño events generally occur at the same time of the year near Christmas. This has been attributed to seasonal locking of the time series, as illustrated by the histogram in panel (b), which shows the monthly positions of unusually warm events (above 1 °C) from the NINO3 data shown in panel (a). Clearly, there is a tendency for El Niño events to occur in boreal winter. The annual cycle therefore represents an intrinsic time scale of the ENSO system.

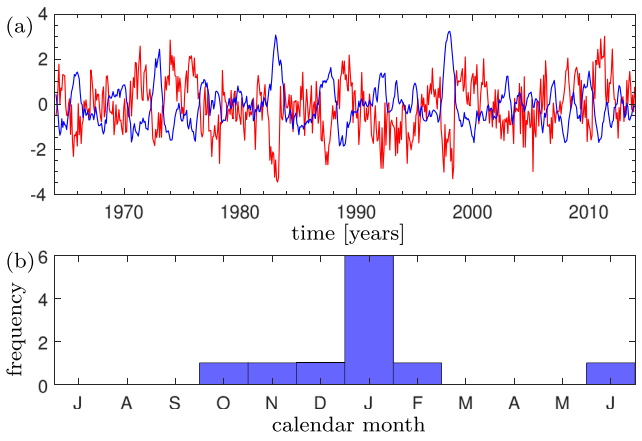


FIG. 1. Panel (a) shows the monthly NINO3 index and SOI deviations from 1964 to 2014 as blue and red curves, respectively. Calendar month locations of warm events (peaks above 1 °C) for the NINO3 index data on panel (a) are displayed in panel (b). The NINO3 data are from NOAA and the SOI data are from the Climatic Research Unit, University of East Anglia.

According to the so-called *delayed action oscillator* (DAO) description of ENSO, which we discuss in detail in Sec. III, certain aspects of the observed SST fluctuations can be attributed to the movement of oceanic waves across the Pacific Ocean. These waves form feedback loops that provide delayed effects to the SST in the eastern Pacific Ocean on the order of months.

When deciding how to describe a given climate system, there are several modelling approaches available, each with their own methodological advantages and challenges. Differences in intrinsic time scales, such as those in the above EBM with ice-albedo feedback, can generally be approximated by ordinary differential equations (ODEs) in the form of fast-slow systems.[59] Transportation phenomena, such as the propagation of oceanic waves in the delayed action oscillator, can be described by partial differential equations (PDEs).

We are concerned here with another modelling approach, which is to represent the delayed effect of feedback loops explicitly. The mathematical model then takes the form of *delay differential equations* (DDEs), where the delay is incorporated explicitly into the relevant feedback term of the equation. This modelling approach is discussed in more detail below in the context of climate models. In the past, it has been applied successfully to a wide range of physical systems; for example, in ecology,[55] control theory,[73] models of genetic regulatory systems,[22,69] neural systems,[11,83] epidemics,[61] coupled chemical oscillators[7] and laser systems.[56,62]

The use of DDEs as equations of choice in conceptual climate modelling has three important advantages. First, the explicit inclusion of delayed effects can potentially lead to a more accurate description of certain processes in the conceptual model. The accuracy of models is often an issue; see, for example, the review Ref. 60 on DDEs in the context of engineering applications. An example from climate science concerns the EBM with ice-albedo feedback discussed above. Earlier literature assumed an instantaneous relationship between albedo strength and global temperatures; for example, see Refs. 33, 63, and 84. Delays were purposely introduced into existing models in an effort to make them more realistic; for example, see Refs. 5 and 34.

Second, a representation of a system by a DDE has the potential to describe the behaviour of interest with a much smaller number of variables and parameters, thus, offering a means of model reduction. In particular, the explicit details of the transportation process itself that underlie a delayed feedback is no longer required as part of the model. Consider, for example, the ENSO system already mentioned above. In order to describe the time evolution of SST anomalies in the eastern equatorial Pacific Ocean, it is sufficient to consider only the effects of the delayed feedbacks in terms of their strengths and the associated delay times. This constitutes a

model reduction compared to the full PDE for zonal wind surface anomaly, surface pressure anomaly, momentum and thermal damping coefficients, etc.

Third, DDEs can be simple enough to be amenable to mathematical analysis, including linear stability analysis and bifurcation analysis with advanced numerical tools. In this context, each delay time appears as a parameter, so that its influence can be investigated systematically.

On the other hand, issues may arise in the justification of certain modelling assumptions. For example, in the vast majority of published studies on DDE climate models, it is assumed that the delays involved remain constant over time, an assumption that is certainly open for debate.

The purpose of this paper is to report how DDEs have been introduced as conceptual models of climate systems, where we focus on EBMs, palaeoclimatology models and ENSO models. We discuss some results from relevant studies, which are, as to be expected, of phenomenological and fundamental nature. We stress that the specific models we consider are the products of other researchers' modelling choices, and we do not attempt to validate them here. Rather, our goal is to review what results can be obtained and, especially, how advanced numerical methods for DDEs can help in this endeavour.

In our review of DDEs in climate models, we focus on DDEs with constant delays, since this is representative of the vast majority of existing literature. Such constant-delay DDEs take the form:

$$\dot{y}(t) = f(y(t), y(t-\tau_1), y(t-\tau_2), \ldots, y(t-\tau_N), t). \qquad (1)$$

Here, $y \in \mathbb{R}^n$ is a state vector and there are $N$ delay terms—one for each feedback loop in the climate system and with a delay $\tau_i$ associated with its underlying physical processes; for example, the time for ice sheets to melt.

There is a well-established theory of DDEs with a finite number of constant delays.[24,40,89,90] In contrast to ordinary differential equations (ODEs) with $n$ variables and phase space $\mathbb{R}^n$, the phase space of the DDE is $C([-\max(\tau_i), 0]; \mathbb{R}^n) \times \mathbb{R}$, where $C([-\max(\tau_i), 0]; \mathbb{R}^n)$ is the infinite-dimensional space of continuous functions over the delay interval with values in $\mathbb{R}^n$ and $t \in \mathbb{R}$ represents time. Therefore, an initial condition for the DDE consists of a whole function segment over the time interval $[-\max(\tau_i) + t_0, t_0]$, often referred to as *initial history*.

The bifurcation theory for constant-delay DDEs is analogous to that for ODEs, because the solutions of constant-delay DDEs depend smoothly on the parameters and initial history and the linearisation of equilibria and periodic solutions have at most a finite number of unstable eigendirections.[28,40] Centre Manifold and normal form reductions can be applied to a constant-delay DDE to yield an ODE that describes the dynamics locally near a given bifurcation. Therefore, one encounters the same type of bifurcation in DDEs as in ODEs. For example, it is known that in the case of negative delayed feedback, $\dot{x}(t) = -g(x(t-\tau))$ for a large family of odd functions $g$, the zero solution undergoes a Hopf bifurcation for a critical value of $\tau$; this creates a family of periodic solutions of period $4\tau$.[15,17,68]

In most cases of past literature on DDEs as conceptual climate models, numerical simulation is employed to investigate their time-dependent solutions. Generally, the existing methods for simulating ODEs can be adapted for DDEs; for example, popular software routines include Matlab's dde23,[86] dde_solver,[95] radar5 (Ref. 39) and the solver of xppaut.[30]

Figure 2 shows example solutions of such a DDE, in this case, the ENSO DDE model (4) introduced in Sec. III B these were computed with the improved Euler method and a constant initial history $h(t) \equiv 0$ to demonstrate different types of dynamical behaviour, which we encounter and discuss in Secs. II–IV in more detail. The model contains two delays, $\tau_p$ and $\tau_n$, and is subject to periodic forcing, representing seasonal effects, with time $t$ measured in years. The solutions are displayed (after transients have died down) as a time series, a projection in the $(h(t), h(t-\tau_p), h(t-\tau_n))$-space, a stroboscopic trace in the $(h(t), h(t-\tau_p), h(t-\tau_n))$-space and a logarithmic power spectrum obtained as the Fourier transform of the time series over 300 years. To obtain a so-called stroboscopic trace,[10,57] the first or head point $h(t)$ of the solution segment is plotted when $t \in \mathbb{N}$ (once for each forcing period) in projection onto the $(h(t), h(t-\tau_p), h(t-\tau_n))$-space.

Row (a) shows a periodic solution of period one. The time series shows periodic motion, which corresponds to a closed curve in the phase space projection. For periodic solutions, the number of points in its stroboscopic trace corresponds to the period of the solution, so this solution is of period one. Finally, the power spectrum has a single dominant peak at one year. Note that all power spectra have a peak at one year due to the seasonal forcing. The solution shown in row (b) is quasiperiodic, which is an unlocked solution on a torus. A slight modulation of local peak heights is not so obvious in the time series; nevertheless, it is clear that the projection of the solution in the $(h(t), h(t-\tau_p), h(t-\tau_n))$-space is not a closed loop but rather a torus, which is filled densely by trajectories. The closed loop formed by the points of the stroboscopic trace is further evidence of a quasiperiodic solution. As such, the distinct peaks in the power spectrum are incommensurate with the frequency of the seasonal forcing. The solution shown in row (c) is periodic, now with a period of four. The solution projection in $(h(t), h(t-\tau_p), h(t-\tau_n))$-space is a closed curve, and there are four points in the stroboscopic trace. In row (d), the solution is chaotic. This is evident from the irregular time series and the broad power spectrum, which contains contributions from all frequencies as is typical for a chaotic solution.

In the context of conceptual climate models, it is generally difficult to estimate or even physically interpret certain parameters, which may realistically be subject to considerable fluctuations over time. Therefore, it is necessary to gain an insight into the possible dynamics of a model across a large range of its parameter space. However, it can be impractical to explore large parameter ranges by numerical integration, because one has to deal with many possible initial conditions, transients and multistabilities. These factors can make it difficult to interpret the model dynamics correctly, understand how typical certain model behaviour is and how certain dynamical features relate to different model components.

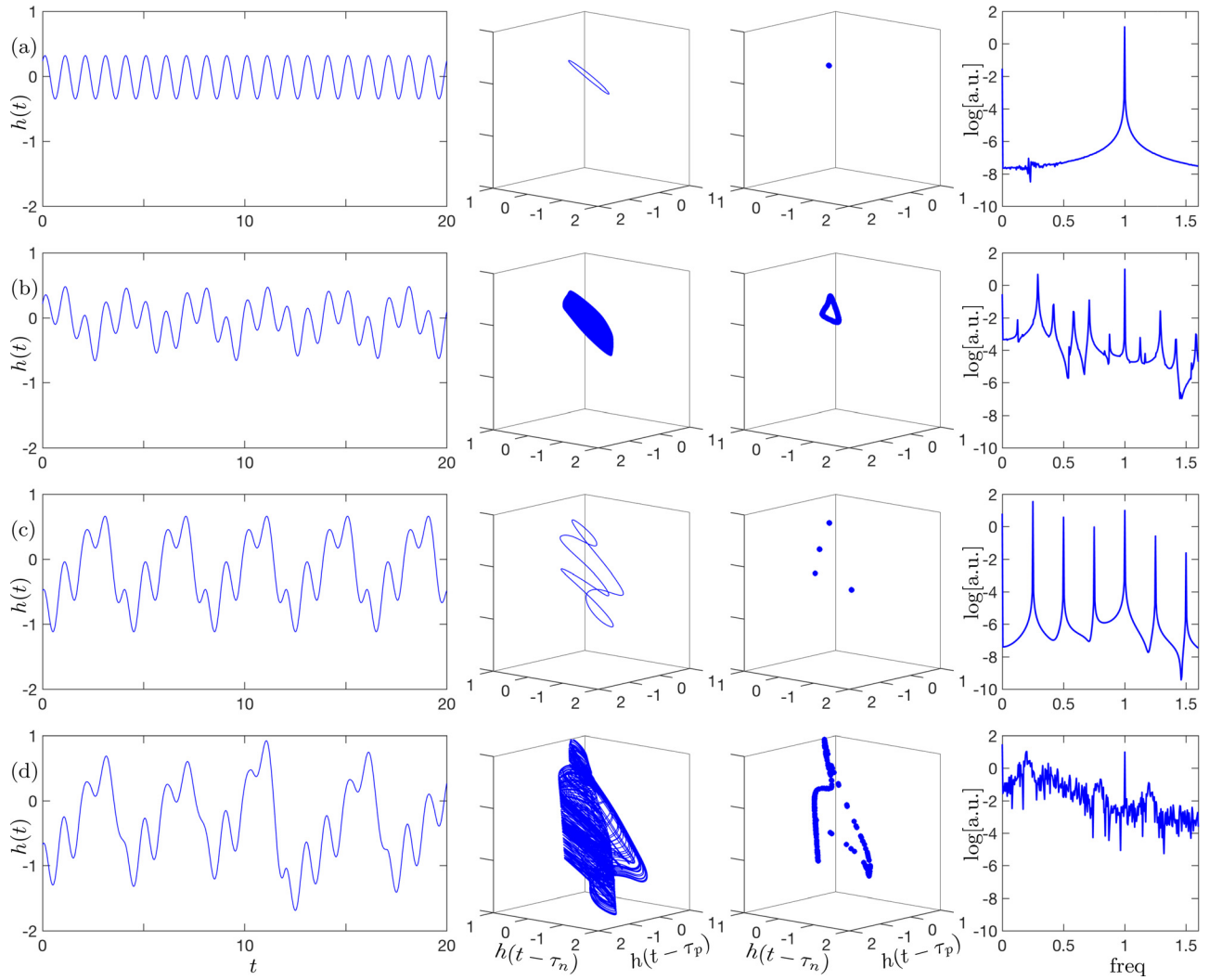


FIG. 2. Stable solutions found by numerical integration of model (4) for $\kappa = 0.9$ (a), $\kappa = 1.2$ (b), $\kappa = 1.5$ (c), and $\kappa = 2$ (d) represented as a time series (far left column), as a projection in the $(h(t), h(t-\tau_p), h(t-\tau_n))$-space (middle-left column), as a stroboscopic trace in the $(h(t), h(t-\tau_p), h(t-\tau_n))$-space (middle-right column) and as a power spectrum on a logarithmic scale in arbitrary units [a.u.] (far-right column). Other parameters are $a = 2.02$, $b = 3.03$, $c = 2.6377$, $d_u = 2.0$, $d_l = -0.4$, $\tau_p = 0.0958$, and $\tau_n = 0.4792$.

One way to overcome these challenges is to employ continuation software, which numerically continues (or tracks) equilibria or periodic solutions, while a parameter is varied. Such software can also calculate the stability of the solutions in order to identify codimension-one bifurcations. These bifurcations, in turn, can be continued numerically as curves in a two-dimensional parameter plane by fixing constraints on the stability of the solutions. Conducting a bifurcation analysis by such means allows one to organise the parameter space into regions of different solution types, providing a comprehensive overview of the dynamical behaviour the model is capable of producing. Continuation methods have been applied to conceptual climate models, but mostly those that do not include delay terms; for example, see Ref. 19 by Crucifix. Impressively, such methods have even been used to analyse a coupled ocean-atmosphere model of a considerably higher complexity level compared to conceptual models; for example, see Ref. 27 by Dijkstra and Neelin.

In this paper, we will see that most results in the existing literature on DDE models of climate systems are obtained by a linear stability analysis of steady-state solutions, simulation of time-dependent solutions and often their spectral analysis. More recent work on these DDE models has utilised state-of-the-art continuation software. Two ready-to-use continuation software packages for DDEs are DDE-Biftool[29,87] and Knut (formerly, PDDE-Cont);[93] the numerical methods implemented in both packages are reviewed in Ref. 77. As we will present and review with some examples, this makes it possible to develop a more detailed and comprehensive picture of possible behaviour of DDE climate models in dependence on parameters. Overall, we suggest that continuation methods provide an efficient means to analyse DDE climate models across appropriately large parameter ranges. We also show that the common modelling assumption that the delays are constant can be relaxed. Indeed, the numerical continuation approach also allows for non-constant delays in DDE climate models (in particular, distributed or state-dependent delays) to be considered.

## II. ENERGY-BALANCE MODELS AND PALAEOCLIMATOLOGY

Ghil and Bhattacharya[34] were the first to incorporate a delay term into a mathematical model of a climate system; in this case, an energy-balance model (EBM). Therefore, we begin our brief review of DDE climate models with the discussion of EBMs. The delay term in this setting was not derived mathematically; rather, it was introduced following previous studies that suggest a time lag between the Earth's surface temperature and the global ice volume; see Ref. 5 and references therein. The best way to model this time lag is subject to choices and debate; we do not attempt to justify the necessary assumptions in this section, but refer the reader to the original papers.

The simplest type of EBM approximates the Earth as a single point in space, and a variable $T$ represents a globally averaged surface temperature. Although mathematically this is a one-dimensional model because it has one variable, in climate science, such a model is conventionally referred to as a *zero-dimensional* EBM because it has no spatial dimensions. Similarly, a one-dimensional EBM has one spatial dimension in the latitudinal (meridional) direction around the Earth, and a two-dimensional EBM is one where the temperature varies across the whole surface of the Earth.

In EBMs, the albedo of the Earth, $\alpha$, parametrises how much solar radiation is reflected back into space by the Earth's atmosphere and surface; thus, given a solar insolation $S$, the power per unit area $S\alpha$ is reflected and $S(1-\alpha)$ is absorbed by the Earth. As described in Sec. I, delayed effects can be incorporated in EBMs by assuming that the albedo of the Earth depends on temperatures in the past.

Some analytical results have been achieved for EBMs with constant-delay DDEs. For example, the hysteresis of fixed point solutions was found in a one-dimensional EBM by Diaz *et al.*[23] and in a two-dimensional EBM by Hetzer.[41–44] Nonetheless, DDE models relevant to palaeoclimatology have primarily been investigated by means of simulation. Various methods of numerical integration have been used; for example, the Euler method with constant initial histories[2] or the Crank-Nicolson finite difference method with initial histories taken from simulated trajectories for zero delay.[5] Often, however, the precise method of integration has not been stated in past literature.

In past literature, simulations were almost always run with the initial histories chosen to be a constant value, which, however, constitutes only a one-dimensional subspace of the space of continuous functions $C$. Note that in Ref. 1, Andersson and Lundberg did compare the use of both constant initial histories and those taken from associated zero-delay simulations, but found that the different initial histories had no effect on their results. However, as we will see later, there are indeed cases where the initial histories used do become important.

Generally, the inclusion of delay effects into EBMs was found to induce surprisingly complicated dynamics, when the dynamics without delay effects was known to be trivial. In Ref. 1, Andersson and Lundberg studied a zero-dimensional EBM of the form:

$$C_0\dot{T}(t) = Q_0[1-\alpha^*(T(t-\tau))] - \sigma g(T)T^4, \qquad (2)$$

where $T$ is the temperature, $C_0$ is the averaged global heat capacity, $Q_0$ is the mean solar radiative input and $\sigma$ is the Stefan-Boltzmann constant. The term $T^4$ appears according to the Stefan-Boltzmann law for black body radiation and the function $g(T)$ is the parametrised effective emissivity coefficient. The function $\alpha^*(T(t-\tau))$ describes how the overall albedo of the Earth depends on temperature with a delay $\tau$, which the authors assume to be constant. They found that for model (2) with a large enough delay, one of the steady-state solutions loses stability, leading to self-sustaining oscillations. As the delay is increased, the dynamics becomes chaotic via a cascade of period-doubling bifurcations.

In Ref. 2, Bar-Eli and Field studied a zero-dimensional EBM with three albedo variables instead of just one, as illustrated schematically in Fig. 3, with $\alpha_c$ and $\alpha_s$ representing the cloud and surface albedos for incoming radiation, respectively. Infra-red radiation emitted from the surface, $L$, has longer wavelengths, so the albedo of clouds for this radiation is different and denoted $\alpha_{cp}$. The authors of Ref. 2 assumed that each albedo is affected by the same constant delay. They observed, similar to Ref. 1, the onset of oscillations and a cascade of period-doubling bifurcations, but also found evidence of an alternative route to chaos that may be related to intermittency.

In a one-dimensional EBM studied by Ghil and Bhattacharya in Ref. 34, the delay describes albedo dependence on continental ice-sheet extension across the globe. These authors demonstrated that varying parameters may lead to the appearance of finite amplitude self-sustaining oscillations without the presence of external forcing; they suggested that this mechanism could play a role in glaciation cycles.

In the context of palaeoclimatology, specific Earth subsystems have also been described by DDEs. The thermohaline circulation in the Atlantic Ocean and its influence on glacial cycles were studied by Ghil *et al.*[35] and then by Wright *et al.*[109] in the framework of discrete space variables as a so-called *Boolean delay equation*. The variable describing the volume of ice sheets in the Northern hemisphere, for example, takes on one of two states: low or high ice volume. This is similar to the discrete variable used in delayed switching.[88]

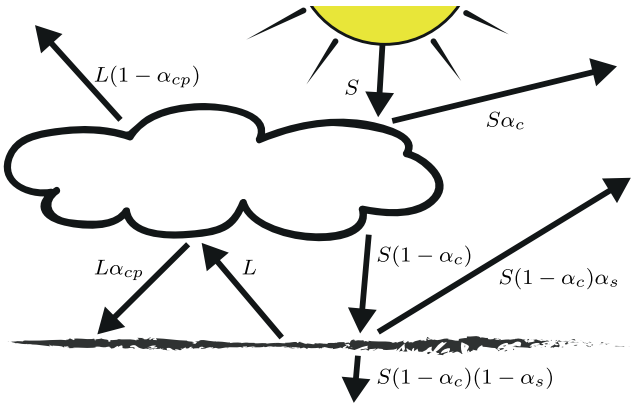


FIG. 3. Schematic representation of the role of albedos, based on the model studied in Ref. 2. $S$ represents solar insolation and $L$ is radiation emitted by the Earth surface. The parameters $\alpha_c$, $\alpha_{cp}$ and $\alpha_s$ are the albedos of the clouds in relation to $S$, the clouds in relation to $L$ and the surface, respectively.

Delays were included in the model of Refs. 35 and 109 due to the gradual expansion of ice sheets and the overturning time of the Atlantic Ocean circulation. It was found by numerical simulation that the length of the glacial episodes depends continuously on the delay parameters and that, depending on the initial history used, the system demonstrates multistability.

In an effort to compare model results with real-world data, Rial and Anaclerio[76] used a DDE to investigate the aspects of the Vostok ice core data, which provide proxy temperature data for the last 430 000 years. Their model is a logistic growth DDE that describes the competition between a positive ice-albedo feedback and a negative delayed precipitation-temperature feedback with a parametrically forced delay time. The latter feedback exists because an increase in the globally averaged temperature induces an increase in precipitation. This allows ice sheets to grow in length towards the equator, increasing the global albedo and thereby decreasing the temperature;[50] for a summary of the feedback mechanisms at play here, see Sec. 11.3 of Ref. 26. Similar to the ice-albedo feedback, the time lag is due to the different time scale at which the ice-sheet changes. A spectral analysis of time series generated with the model for different forcing strengths of the delay time showed similarities to the ice core data.[76] A similar version of the logistic growth DDE was coupled to a simple energy-balance equation by Rial in Ref. 75. Time series and power spectra from this model captured significant features from deep-sea sediment and ice core data at Milankovitch and millennial scales, including the characteristic saw-tooth shape of the data time series, the mid-Pleistocene climate switch and the Dansgaard-Oeschger oscillations. Generally speaking, the results suggested that the Earth's climate may be only weakly driven by astronomical forcing with most "intriguing" dynamical features being the result of internal nonlinear processes and feedback mechanisms.

## III. DELAYED ACTION OSCILLATOR MODELS OF ENSO

Conceptual ENSO models have been developed that focus on the interactions of key mechanisms in order to better understand some basic dynamical features, such as those described in Sec. I. Most of these models are based on the so-called delayed action oscillator (DAO) paradigm, first introduced in 1988 by Suarez and Schopf.[92] In this paradigm, ENSO dynamics are driven by feedback loops that form through the coupling of atmospheric and oceanic processes above and in the equatorial Pacific Ocean, as illustrated in Fig. 4. The variable $h$ represents deviations of the thermocline depth from its long-term mean at the eastern boundary of the equatorial Pacific Ocean. The thermocline is a relatively thin layer of the ocean that separates the deeper cold waters from the warmer well-mixed waters. Its depth can be considered a proxy for sea-surface temperature (SST), so a large $h$ corresponds to the warming of the eastern equatorial Pacific Ocean observed during El Niño events. A positive perturbation in $h$ slows down the easterly trade winds, creating westerly wind anomalies, as shown in Fig. 4. This induces a transport of warm surface water in the central part of the Pacific Ocean, where the ocean-atmosphere coupling is

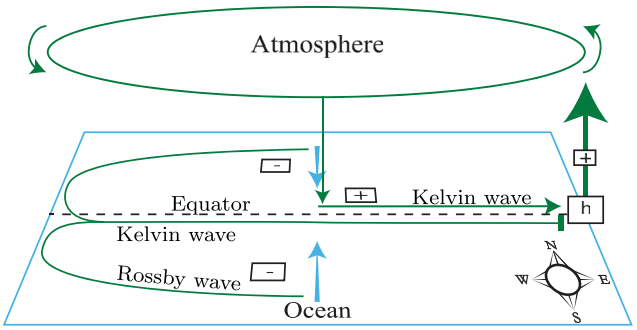


FIG. 4. The variable $h$ represents deviations from the mean thermocline depth at the eastern boundary of the equatorial Pacific Ocean. A positive perturbation in $h$ creates westerly wind anomalies. The coupling between the ocean and the atmosphere allows for the creation of positive and negative delayed feedbacks. The green arrows and bars represent processes of positive and negative reinforcement, respectively (see text for details).

the strongest. Because of the so-called Ekman transport phenomenon, the surface water moves towards the equator (that is, perpendicular to the wind anomaly direction), as indicated by the blue vertical arrows in Fig. 4; for details, see Chap. 3 of Ref. 100. The SST rises, creating a positive signal that is carried back to the eastern boundary as a so-called Kelvin wave to form a positive feedback loop. Simultaneously, a negative signal is created off the equator, where there is a deficit of warm surface water. This signal travels westward as a so-called Rossby wave, which is then reflected at the western edge of the Pacific basin before travelling back to the eastern boundary as a Kelvin wave, thus closing the negative feedback loop represented by the bar in Fig. 4. In this system, the delays are due to the finite speeds of the Kelvin and Rossby waves, which typically take 1–6 months to carry a signal across the Pacific Ocean.

As mentioned above, in the DAO models that we discuss below, the variable $h$ describes anomalies of the thermocline depth, which is considered a proxy for SST, in the eastern equatorial Pacific Ocean. A modelling assumption made in all the DAO models is that the delay times associated with the travelling oceanic waves are constant. The models were generally studied by simulations; for example, with a variable-order, variable-step Adams method[32,99] or a forward-stepping algorithm (Appendix 1 of Ref. 79), but in many cases, the precise integration method was not stated. Nonetheless, the use of constant initial histories seems to be common practice when running simulations (except for Refs. 52–54).

In contrast to the case of EBMs and palaeoclimatology models, the justification of describing the ENSO system with DDEs has a strong physical background. To explain why this is so, we briefly discuss the Zebiak-Cane model.[111] It is classified as an intermediate complexity model (ICM)—a type of model that on the scale of complexity lies in-between GCMs and conceptual models. ICMs utilise the same physical equations as GCMs, but apply them only to a subsystem of the global climate together with artificial boundary conditions. The Zebiak-Cane model, for instance, combines Newton's laws of motion to describe fluid flow with the laws of thermodynamics to describe the coupled dynamics of the ocean and atmosphere of the tropical Pacific Ocean. Specifically, the equations represent only anomalies from a seasonally

varying mean state, which is specified by observational data. Compared to typical numerical weather-prediction models, the Zebiak-Cane model is still considered simple. Despite its relative simplicity, it was shown to be very good at predicting the timing and magnitude of El Niño events.[13]

By following assumptions made by Jin in Ref. 46, one can derive equations for the propagation of Kelvin and Rossby waves from the Zebiak-Cane model. By applying appropriate boundary conditions, one can then represent the resulting feedback loops as described above by a DDE. Hence, many of the assumptions required for the DDE description of ENSO dynamics are justified, at least indirectly, by the success of the Zebiak-Cane model. Details of the DDE derivation can be found in Chap. 7.5.4 of Ref. 25.

### A. Basic DAO with delay

The story of investigating ENSO by means of DDE models begins with a DAO model introduced by Suarez and Schopf in Ref. 92, which is given by

$$\dot{h}(t) = h(t) - h(t)^3 - \alpha h(t-\tau). \tag{3}$$

The first term reflects a "local" (instantaneous) positive feedback, whereby a SST perturbation heats the atmosphere, whose wind response drives ocean currents to reinforce the original perturbation. The growth of the instability due to the positive feedback is limited by effects such as advective processes in the ocean and moist processes in the atmosphere, which are represented by the second term in Eq. (3). The third term describes the effect of delayed oceanic waves. A linear stability analysis of this simple model was conducted in Ref. 92 to show that the steady-state solution loses stability for certain parameter values of $\alpha$ and $\tau$. The resulting periodic solutions have periods of at least twice the length of delay, demonstrating that this simple feedback can provide a mechanism for ENSO's oscillatory behaviour on an appropriate interannual timescale.

In Ref. 4, Battisti and Hirst showed that model (3) can be derived from an intermediate coupled ocean-atmosphere model[3] that is very similar to the Zebiak-Cane model. Through their derivation of the DDE, Battisti and Hirst were able to relate the parameters to background states of the ocean and atmosphere and the geometry of the Pacific basin. By comparing alternative background states and geometries, the results helped to explain why ENSO-like variability is not observed in the tropical Indian or Atlantic Ocean. Supporting evidence of the DAO paradigm was provided by empirically derived time-delay models, which were shown to produce oscillations similar to observable data by Graham and White in Ref. 37 and to a sophisticated oceanic general circulation model by Schneider *et al.* in Ref. 82.

### B. Multiple feedback loops and seasonal forcing

The simple negative delayed feedback in model (3) provides a mechanism for SST oscillations. There have been numerous extensions to this model, in an effort to make the models more realistic by including additional time-scales. For example, the inclusion of only one delay term is due to the modelling assumption that only one mode of Rossby wave is important. In fact, many modes of Rossby waves form at different latitudes with different phase speeds. White *et al.*[107] showed, by simulation and spectral analysis of a DAO model, that delay times associated with sets of Rossby waves forming at approximately 7°N, 12°N, and 18°N result in biennial, interannual and decadal signals similar to those observed in data by Tourre *et al.*[96]

The positive delayed feedback formed by Kelvin waves, as described above, and seasonal forcing were included by Tziperman *et al.* in Ref. 99 in the DDE model

$$\begin{aligned}\dot{h}(t) &= aA(\kappa, h(t-\tau_p)) \\ &\quad - bA(\kappa, h(t-\tau_n)) + c\cos(2\pi t),\end{aligned} \tag{4a}$$

$$\text{with } A(\kappa,h) = \begin{cases} d_u \tanh\left(\dfrac{\kappa}{d_u}h\right) & \text{if } h \geq 0, \\ d_l \tanh\left(\dfrac{\kappa}{d_l}h\right) & \text{if } h < 0. \end{cases} \tag{4b}$$

The positive and negative feedbacks are associated with fixed delay times, $\tau_p$ and $\tau_n$, respectively. The seasonal forcing is represented by additive forcing with a period of one year. The function $A(h)$ is a special case of the ocean-atmosphere coupling function justified in Ref. 65 with coupling strength $\kappa$ and horizontal asymptotes $d_h > 0$ and $d_l < 0$.

The model (4) is significant because it demonstrated that the irregularity characteristic of ENSO could be reproduced as chaotic behaviour of this simple DDE. Note that there is a competing theory that the irregularity is driven by noise, in particular, by small-scale, high-frequency stochastic forcing; for example, see Refs. 70 and 94. Specifically, Tziperman *et al.* observed a transition to chaos upon increasing the parameter $\kappa$ and presented the same solutions shown here in Fig. 2. Based on these solutions, these authors suggested that the chaotic behaviour at $\kappa = 2.0$ was due to the coexistence of mode-locked solutions or, in other words, overlapping resonances. Furthermore, they suggested that the coexistence of different mode-locked solutions depends on the strength of nonlinearity in the model, so that $\kappa$ must be sufficiently large to observe irregular behaviour. The view that ENSO irregularity is primarily due to low-order chaotic processes gained further support from Saunders and Ghil in the study of a different DAO model with two fixed delay times and a seasonal cycle.[79]

Ghil *et al.* considered a simplification of model (4) in Ref. 36, here referred to as the Ghil-Zaliapin-Thompson model, with $a = 0$, $d_u = 1$ and $d_l = -1$ that focuses on the interaction between the negative delayed feedback and the seasonal forcing. Model (4) thus becomes:

$$\dot{h}(t) = -b\tanh(\kappa h(t-\tau_n)) + c\cos(2\pi t). \tag{5}$$

Despite its simplicity, the Ghil-Zaliapin-Thompson model (5) demonstrated complicated dynamics; specifically, it reproduced important ENSO features such as intraseasonal oscillations, interdecadal variability, frequency locking for varying parameters (observed as a Devil's terrace or two-dimensional Devil's staircase), as well as phase locking with

the seasonal forcing. A primary tool utilised by Ghil *et al.* was the computation of the so-called *maximum maps*, which plot the maxima of simulated solutions as a function of two parameters. In order to avoid transient effects, a trajectory is given sufficient time (thousands of years) to approach and reach a stable attractor. To ensure accuracy, the length of time from which the maximum was obtained needed to be sufficiently long, because the solution may not necessarily be periodic.

Figure 5 shows an example of a maximum map from Ref. 36 with parameters $c$ and $\tau_n$ and a single fixed initial history of $h(t) \equiv 1$. One can easily identify two regimes—one in the upper-left and one in the lower-right side of the parameter plane—divided by a sharp interface, which represents where there is a rapid transition in $\max[h(t)]$. Further sharp interfaces form elongated shapes in the upper-left side of the parameter plane. Given that generic stable solutions to the model depend continuously on the parameters and the initial history, as proven in Ref. 36, the observed sharp interfaces imply the existence of stability loss and families of unstable solutions.

The existence of multistabilities in model (5) was uncovered in a follow-up paper to Ref. 36 by studying the effect of different constant initial histories.[110] Zaliapin and Ghil also demonstrated in Ref. 110 that the phase locking observed in Ref. 36, which is an important feature of the model because it agrees with the tendency of El Niño events to occur primarily towards the end of the calendar year, is a robust feature of the model, except when the forcing is weak.

In Ref. 98, Tziperman *et al.* studied the phase locking mechanism with the model

$$\begin{aligned} \dot{h}(t) &= aA(\kappa(t-\tau_p), h(t-\tau_p)) \\ &\quad -bA(\kappa(t-\tau_n), h(t-\tau_n)) - eh(t), \\ \kappa(t) &= k_0 + d_k \sin\left(\frac{\pi}{6}t\right) \end{aligned} \tag{6}$$

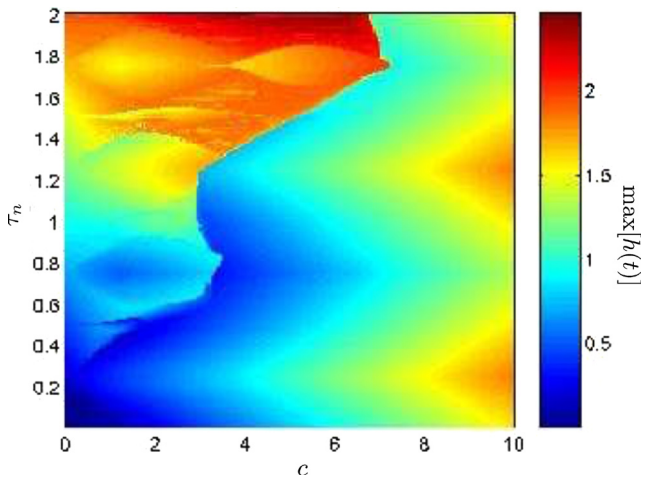


FIG. 5. Maximum map of the Ghil-Zaliapin-Thompson model (5) displaying the maximum value of $h(t)$ according to the colour scheme in the $(c, \tau_n)$-plane. Parameters are $b = 1$ and $\kappa = 11$, and the initial history is $h(t) \equiv 1$; $t \in [-\tau_n, 0]$. Reproduced with permission from Ghil *et al.*, Nonlinear Processes Geophys. **15**, 417–433 (2008). Copyright 2008 CC-BY licence.

with $A(\kappa, h)$ given by Eq. (4b). The last term of the DDE reflects attenuation due to dissipation. Motivated by studies of more complex models, the effect of the seasons was not included as an additive term, but as parametric forcing of the ocean-atmosphere coupling strength. The parameters $k_0$ and $d_k$ are the mean coupling strength and annual variation, respectively. Time $t$ is measured in months. Tziperman *et al.* analysed a particular solution of model (6) that demonstrated non-periodic behaviour with large extrema of varying size occurring every three years. They showed that for this solution, the El Niño events can only reach their peak when the coupling strength is at its minimum strength, which is at the end of the calendar year, and that this mechanism is very robust to parameter changes. This phase-locking mechanism was later shown by Galanti and Tziperman in Ref. 32 to be essential in a more sophisticated model, which took the form of an ODE coupled to a delay-difference equation, derived from the Zebiak-Cane model by following similar physical assumptions as Jin in Refs. 45 and 46. This model retains the use of constant delays, but incorporates damping terms and oceanic wave reflections not only at the western, but also at the eastern boundary of the Pacific Ocean.

### C. Continuation results for model (6)

In order to gain a more comprehensive view of the possible dynamics of model (6) and confirm the observations made in Ref. 98, Krauskopf and Sieber[58] employed the continuation software DDE-Biftool to conduct a bifurcation analysis in the $(d_k, k_0)$-plane. Figure 6 illustrates that there are qualitative changes in solutions, which occur as parameters pass through curves of torus bifurcations (TR), period-doubling bifurcations (PD) and saddle-node bifurcations of periodic orbits. In the autonomous case of $d_k = 0$, the trivial zero-solution loses stability at a Hopf bifurcation (H) and

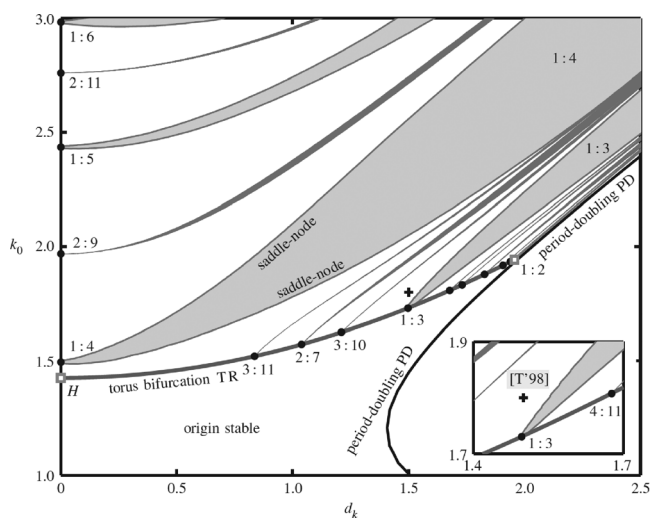


FIG. 6. Bifurcation set of model (6) in the $(d_k, k_0)$-plane. Curves of torus (TR) and period-doubling (PD) bifurcations are shown. Saddle-node bifurcations of periodic orbits form the boundaries of $p$:$q$ resonance tongues. The inset is an enlargement to highlight the location of the parameters used in Ref. 98. Other parameters are $a = 0.2535$, $b = 0.1901$, $e = 0.1601$, $d_u = 3$, $d_l = -1$, $\tau_p = 1.15$ and $\tau_n = 5.75$. Reproduced with permission from B. Krauskopf and J. Sieber, Proc. R. Soc. A **470**, 348 (2014). Copyright 2014 Published by the Royal Society.

creates a family of periodic orbits. Once the forcing is introduced with $d_k > 0$, the zero-solution becomes a trivial periodic solution with an amplitude of zero and a period of one, which remains stable for small $k_0$ and $d_k$. While increasing $d_k$, the trivial periodic solution loses stability in a period-doubling bifurcation, creating period-2 solutions. On the other hand, increasing the parameter $k_0$ leads to stability loss through torus bifurcations. Therefore, above the curve TR, there exist invariant tori and associated $p$:$q$ resonance tongues, as labelled in Fig. 6, for all $q \leq 11$. The resonance tongues, which are bounded by curves of saddle-node bifurcations of periodic orbits, contain families of stable and saddle $p$:$q$ periodic orbits that are frequency locked. Therefore, within each resonance tongue, the invariant torus has a fixed rational rotation number $p/q$. In-between the resonance tongues, quasiperiodic solutions exist.

It should be noted that theory predicts the existence of an infinite number of resonance tongues, one for every rational rotation number of the torus, which become increasingly narrow with increasing $q$. Figure 6 demonstrates that one can obtain an effective overview of all possible dynamics of model (6) for a relevant range of parameters. The insert in the lower-right corner of Fig. 6 is an enlargement of the parameter plane near the root point of the 1:3 resonance tongue. The cross indicates the parameters used by Tziperman *et al.* in Ref. 98 and reveals why the solution to model (6) demonstrated aperiodic motion, yet closely resembled a period-three periodic orbit. Krauskopf and Sieber also plotted all stable 1:3 and 1:4 solutions (not shown) from the parameter range considered in Fig. 6 in order to show that the phase locking to the seasonal cycle is indeed a robust feature, in agreement with the claim made in Ref. 98.

### D. Continuation results for model (5)

In Ref. 53, we used DDE-Biftool to conduct a bifurcation analysis of the Ghil-Zaliapin-Thompson model (5) studied in Refs. 36 and 110. Figure 7 shows maximum maps overlaid with a bifurcation set in the $(c, \tau_n)$-plane; white, grey and black curves represent saddle-node bifurcations of periodic orbits, period-doubling bifurcations and torus bifurcations, respectively. In contrast to the maximum map shown in Fig. 5, which was calculated for a single fixed initial history, the maximum maps in Fig. 7 are calculated such that for each row of fixed delay $\tau_n$, the parameter $c$ is scanned up and down (using previous solutions as initial histories), as indicated by the arrows. This convenient and systematic approach means that the simulated trajectory stays on the same branch of solutions, while $c$ is slowly varied until stability is lost. Comparing panels (a) and (b) of Fig. 7, the maximum maps reveal regions of bistability, where the maxima of observed solutions depend on the direction in which the parameter $c$ is varied.

The bifurcation set in Fig. 7 divides the $(c, \tau_n)$-plane into regions of different solution types. Generally, the dynamics is driven by two independent mechanisms that create self-sustaining oscillations: the negative delayed feedback and the seasonal forcing. Along the line $c = 0$ in Fig. 7, the periodic orbits depend only on the negative delayed

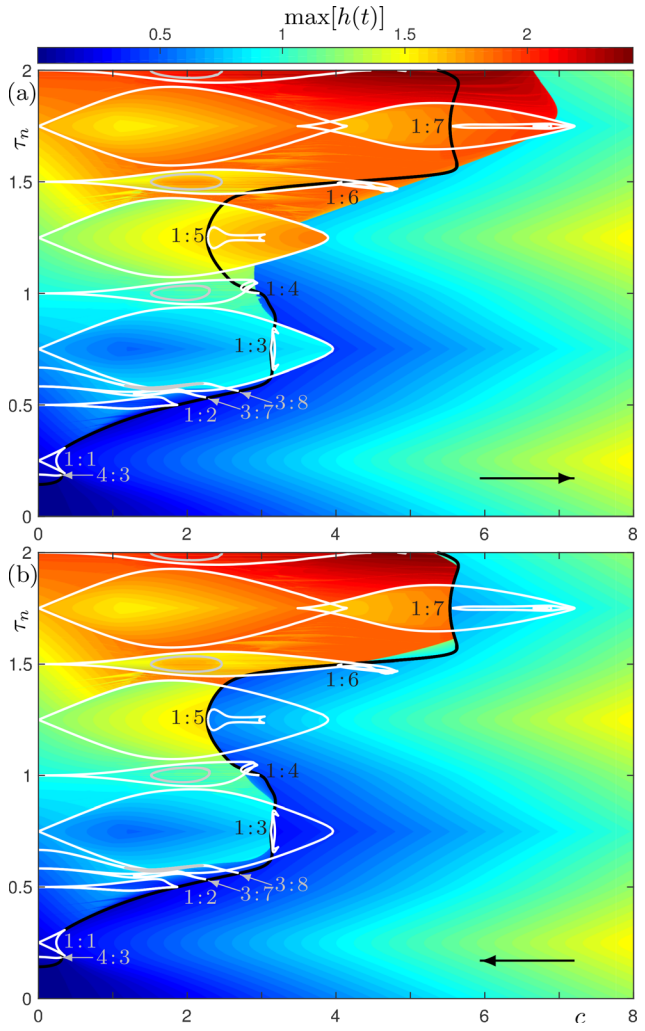


FIG. 7. Maximum maps of the Ghil-Zaliapin-Thompson model (5) with curves of saddle-node bifurcations of periodic orbits, period-doubling and torus bifurcations; drawn in white, grey and black, respectively. Several frequency ratios of resonance tongues are indicated. Other parameters are $b = 1$ and $\kappa = 11$.

feedback term, creating periodic solutions for $\tau_n > \pi/(2\kappa)$.[15,17,68] On the other hand, solutions with large $c$ are dominated by the seasonal forcing, so that they all have a period of one and appear sinusoidal-like. As the parameter $c$ is decreased in panel (b), those solutions lose stability in torus bifurcations at the black curve. Therefore, between line $c = 0$ and the black curve of torus bifurcations is a region where both oscillations interact and give rise to dynamics on an invariant torus. The locked solutions on the torus are organised into resonance tongues, which appear as elongated shapes in Figs. 5 and 7.

The sharp interfaces of the maximum maps in Fig. 7 that could not be explained by bifurcations of periodic orbits are shown in Ref. 53 to be more complicated bifurcations involving folding tori. These folding tori were analysed in detail in Ref. 52, and were shown to possess a complicated bifurcation structure that occurs as tori approach each other and break-up. As briefly demonstrated in Ref. 52, this phenomenon can be considered as a mechanism for climate tipping that, in contrast to simple fold bifurcations of equilibria or periodic orbits, has the additional bifurcation structure

associated with folding tori that could offer precursor information about an approaching tipping point. This result is a good example of how new phenomena, which are easily overlooked in complex models, can be found and studied in conceptual models.

### E. Continuation results for model (4)

The combination of continuation software with bifurcation theory was applied to model (4) in Ref. 54. Although it was a crucial result that this simple deterministic model could produce irregular behaviour reminiscent of real-world data, there remained important open questions: Is this behaviour characteristic of the model? In other words, how robust is this behaviour to changes in parameters? By what mechanism does the solution become chaotic?

Figure 8 addresses these questions; it shows a bifurcation set in the $(c, \kappa)$-plane with curves of saddle-node bifurcations of periodic orbits (blue), torus bifurcations (red), and period-doubling bifurcations (black). The maximal Lyapunov exponent of each solution, in cases where it is positive indicating chaotic behaviour, is displayed by a colour scheme. The maximal Lyapunov exponents are calculated according to the algorithm for DDEs described in Ref. 31. Also shown in Fig. 8 are the parameter points of solutions (a)–(d) referred to by Tziperman *et al*. in Ref. 99 and displayed in Fig. 2.

In Fig. 8, we see a (red) curve of torus bifurcations for small values of $\kappa$ and resonance tongues that are rooted at the zero-forcing line $c = 0$. For clarity, we only show 1:$q$ resonance tongues rooted at the $c = 0$ line (and not the resonance tongues emerging from the red curve of torus bifurcations). We found in Fig. 8 that positive maximal Lyapunov exponents appear due to overlapping resonance tongues via

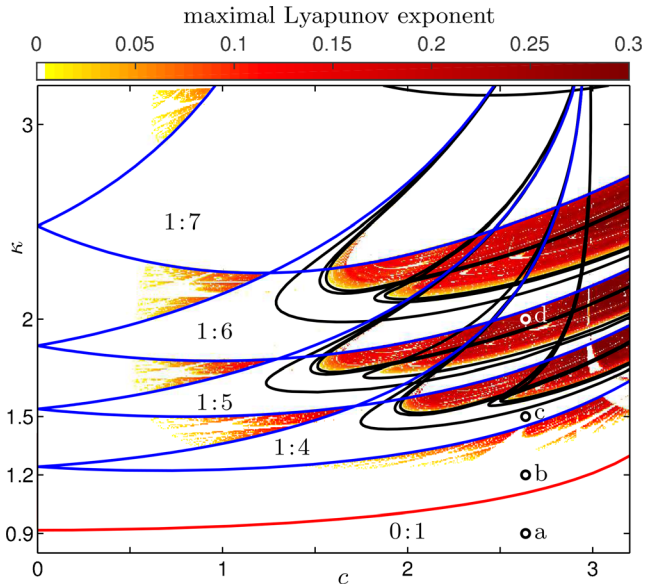


FIG. 8. Bifurcation set of model (4) in the $(c, \kappa)$-plane with saddle-node bifurcations of periodic orbits (blue), torus bifurcations (red), and period-doubling bifurcations (black). The shown $p$:$q$ resonances are labelled, similar to the points (a)–(d) corresponding to solutions considered in Ref. 99 and shown in Fig. 2. The colour scheme indicates the positive maximal Lyapunov exponent. Other parameters are $a = 2.02$, $b = 3.03$, $d_u = 2.0$, $d_l = -0.4$, $\tau_p = 0.0958$, and $\tau_n = 0.4792$.

cascades of period-doubling bifurcations. This is also true for regions outside of the displayed resonance tongues because in-between those that are shown exist smaller, higher-order resonance tongues that overlap.

The parameter point of solution (a) in Fig. 2 is located in the parameter region of Fig. 8 that is dominated by the seasonal forcing; hence, it is a solution of period 1. Upon increasing $\kappa$ for fixed $c = 2.6377$, the solution loses its stability at a torus bifurcation, so that quasiperiodic can also be observed. The parameter point of solution (b) is not inside any resonance tongue, and is therefore observed in Ref. 99 to be quasiperiodic. On the other hand, the parameter point corresponding to solution (c) lies within the 1:4 resonance tongue, in agreement with the period-4 solution seen in Ref. 99. The chaotic solution (d) in Fig. 2 is situated in a parameter region of overlapping resonance tongues in Fig. 8. Furthermore, according to the bifurcation set, the same changes of solution type will be observed while increasing $\kappa$ for any fixed $1.5 \lesssim c \leq 3.2$ and possibly for larger $c$, albeit for different values of $\kappa$. Therefore, the transition to chaos observed by Tziperman *et al*. and illustrated in Fig. 2 is indeed a prominent feature of model (4) and leads to chaotic behaviour across a substantial range of parameters.

Figure 9 shows the time series of solution (d) over a longer time window. It is a good example to demonstrate how simple feedback mechanisms can account for the irregularities observed in both the amplitude and the frequency of El Niño events.

Particular routes to chaos that account for the irregular behaviour in ENSO models have been discussed at length; for example, in literature reviews.[74,78,102] In various ENSO models, routes to chaos have been identified as either the quasiperiodic route,[49,97,98] period-doubling route[12,16,65] or the intermittency route.[104] Interestingly, it was shown in Ref. 54 that different routes to chaos can coexist, even to the same chaotic solution, depending only on the chosen path through parameter space. While increasing $\kappa$ in model (4) leads to chaos via the period-doubling route, an alternative route to the same chaotic attractor is found when decreasing $\kappa$ for a fixed $c$. In this case, chaos appears just below the lower boundary of the 1:6 resonance tongue seen in Fig. 8. After exiting the 1:6 resonance tongue, as $\kappa$ is decreased, episodes of periodic behaviour become increasingly shorter until they apparently disappear. This is evidence of the so-called intermittent transition,[72] which is characterised by the sudden appearance of chaos at a saddle-node bifurcation.

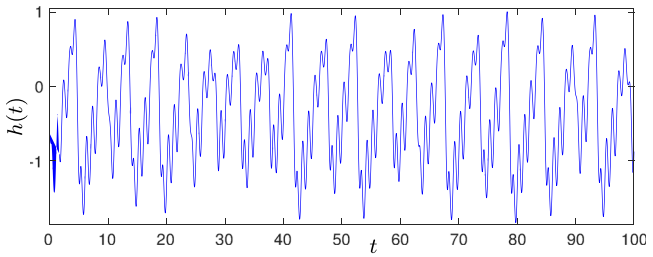


FIG. 9. Time series found by numerical integration of model (4) for $a = 2.02$, $b = 3.03$, $c = 2.6377$, $d_u = 2.0$, $d_l = -0.4$, $\tau_p = 0.0958$, $\tau_n = 0.4792$, and $\kappa = 2.0$.

Notice that many aspects of the bifurcation set in Fig. 8 are similar to that of Fig. 6. One difference between the two is that, while the resonance tongues in Fig. 8 overlap each other, the resonance tongues in Fig. 6 appear to only approach each other without overlapping. Whether this reflects a difference between additive and multiplicative forcing, or whether the resonance tongues in Fig. 6 do overlap for larger parameter values than those considered is not clear and warrants further analysis.

### F. Alternative ENSO paradigms

Apart from the DAO paradigm, other ENSO paradigms have been considered and modelled as DDEs. The so-called western Pacific oscillator paradigm focuses on the competition between central equatorial and western off-equatorial Pacific thermocline and demonstrates the potential importance of western Pacific variability in relation to ENSO. It is introduced by Weisberg and Wang in Ref. 105 and modelled by a set of four DDEs with four variables describing anomalies in: equatorial thermocline depth in the eastern Pacific Ocean, off-equatorial thermocline depth in the western Pacific Ocean and the zonal wind stresses above the west-central and western Pacific Ocean. The thermocline variables depend on delayed wind stresses, modelled with two fixed delays. Weisberg and Wang showed that neither delays nor nonlinear terms are necessary to produce oscillations. Although the oscillations are periodic, Weisberg and Wang argued that irregularities could be introduced into the dynamics by, for example, adding nonlinearities or stochastic forcing to the model. This study inspired Wang *et al.* to further investigate the role of western Pacific variability in a more complex model related to the Zebiak-Cane model in Ref. 103, which produced co-oscillating anomaly patterns in the western and eastern Pacific Ocean that were consistent with observations.

In Ref. 101, Wang derived a DDE model that encapsulates four different ENSO paradigms: the DAO, the western Pacific oscillator, the recharge-discharge oscillator[45,46] and the advective-reflective oscillator.[71] The model consists of four variables describing anomalies in: the average SST in the eastern equatorial Pacific Ocean, the off-equatorial thermocline depth in the western Pacific Ocean, and the zonal wind stresses above the central and western equatorial Pacific Ocean. Wang suggested that naturally varying parameters could alter the relative role of each paradigm in different El Niño and La Niña events. For example, the western Pacific oscillator might play a larger role in strong El Niño events, since strong equatorial wind anomalies are known to occur in the western Pacific Ocean at times of strong El Niño events.

## IV. DISCUSSION AND OUTLOOK

In this paper, we reviewed how DDEs have been introduced into climate models. In order to reflect the balance of existing literature, we chose to focus on the application of DDEs to EBMs, palaeoclimatology and ENSO models. Upon including delayed effects into the respective phenomenological models, the dynamics becomes considerably more complicated and allows for the reproduction and investigation of certain dynamical features that are observed in nature. For example, a phase locking mechanism is identified as a possible explanation why El Niño events tend to occur around Christmas. Most of the results have been achieved by running simulations. We, therefore, highlighted some more recent results that were obtained by continuation methods that are able to deal effectively with multistabilities, transients and the difficulty of choosing appropriate initial conditions. These reviewed results include the identification of folding tori, which are particularly interesting in the context of climate tipping, as well as clarification of the precise mechanism by which chaotic behaviour was observed in simulations of an ENSO model.

Beyond the focus of this brief review, DDEs have been used to describe other climate systems; these include an interdecadal cycle in the Arctic and Greenland Sea,[20] an interdecadal cycle in the subpolar North Atlantic,[108] vegetation interaction with global climate fluctuations,[21] heat transport between the Pacific extratropics and tropics,[38] rainfall with land-atmosphere coupling through soil moisture, vegetation and surface albedo[6] and boundary reflections of oceanic waves in the Indian Ocean.[106] Furthermore, we have considered deterministic models here, yet stochastic behaviour is undoubtedly present in climate systems and could have highly relevant effects, even if a system is primarily driven by deterministic processes. For example, Stone *et al.*[91] added an additive Gaussian white noise term to the DDE model (4) in order to investigate the effects of noise on the DAO. For some values of the parameters, it was shown that the noise affects the type of observed solution; in particular, noise can induce chaotic behaviour for parameters otherwise associated with periodic or quasiperiodic behaviour. A feature of the resulting time series is "regime like behaviour" with periods of both large amplitude erratic oscillations and small amplitude annual cycles, similar to the dynamics seen in more complex ENSO models.[14] How best to represent noise in a conceptual model is not clear. Modelling choices include whether the stochastic effects are additive or multiplicative, and which distribution is most appropriate. One could assume Gaussian white noise, as in Ref. 91, but this may not be an accurate representation, since the noise may be subject to various nonlinear processes. For further examples of DDE climate models with noise, see Refs. 6, 38, 80, and 106.

### A. Feedback loops with nonconstant delays

We now briefly discuss nonconstant delays in DDE climate models—a subject we believe has considerable potential for rendering phenomenological models more realistic and relevant from a climate modelling point of view. Moreover, DDEs with nonconstant delays are presently a research area of considerable interest from a dynamical systems point of view, and climate DDEs arise as natural test-bed models for new theory and numerical approaches.

A first class of nonconstant delays, referred to as *distributed* or *weighted* delays, describes the situation that a variable might depend on a range of past times. Then, the delay

term $y(t-\tau_i)$ becomes an integral term $\int_0^{\tau_{max}} w(\tau)y(t-\tau)d\tau$, where values of $y$ are considered over a delay range of $[0, \tau_{max}]$ and $w(\tau)$ is the associated kernel or delay distribution that says how different past times contribute to the overall feedback. In the literature on DDE climate models, distributed delay was considered in a very early publication by Bhattacharya *et al*.[5] Despite this, the trend towards the use of a constant delay term quickly set in, because it simplifies the analysis of the DDE. In fact, the study of the constant-delay DDE serves as a starting point for any investigation of the role of nonconstant delays, but we believe it to be promising and necessary that future work reconsiders the use of distributed delays in climate models. For example, in the above mentioned DDE ENSO models, the delays are always assumed to be constant, while oceanic wave velocities are distributed around mean velocities.[8] It would be interesting to include into the model the associated distribution of delays, which is influenced in no small part by the geometry of the Pacific basin near the equator.

A second type of nonconstant delay arises when a delay depends on the state of the system itself, which leads to a delay term of the form $\tau_i = \tau_i[t, y(t)]$; one speaks of *state-dependent delays*. For example, the delays in the DAO paradigm of ENSO are determined in part by the position in the Pacific Ocean where the oceanic waves form, which is influenced by the position of the western Pacific warm-pool. Yet, the position of the warm-pool itself is influenced by changes in the thermocline depth. An implicit expression for a state-dependent delay in this context has already been suggested by Clarke *et al*. in Ref. 18.

State-dependence also arises when taking into account subsurface ocean adjustment dynamics. In a series of papers,[47,48,66,67] Neelin and Jin studied three regimes of ENSO dynamics: the fast-SST regime, where the SST adjustment to changes in thermocline depth is instantaneous; the fast-wave regime, where the speeds of oceanic waves are infinite; and the mixed-mode regime, where both SST adjustment and oceanic wave propagation times are essential. They showed that the mixed-mode regime is the most realistic. Although the coupling between deviations in the thermocline depth and SST is considered in the DDE model derivation for the DAO paradigm (for example, see Refs. 4 and 46), it is also interesting to consider how this relationship affects the nature of the delay itself. One could incorporate the SST adjustment time by adding an additional delay time that will depend on the position of the thermocline itself. As a quite simple example, we consider linear state-dependent delays, of the positive and negative feedback loops, of the form

$$\bar{\tau}_{p/n}(t) = \tau_{p/n} + \eta\, h(t). \tag{7}$$

It represents the respective overall delay as the delay of the oceanic wave dynamics $\tau_{p/n}$ plus the time $\eta h(t)$ required for the upwelling process to carry the signal from the thermocline to the sea surface. The parameter $\eta$ represents the inverse of the speed of the upwelling process, as well as the strength of the state-dependence of the delay. Assuming that $h$ is scaled, such that the distance between the mean thermocline depth and the sea surface in the eastern equatorial Pacific Ocean is approximately 1, $\eta = 0.04$ corresponds to a SST response time of about two weeks, as estimated in Ref. 112.

DDEs with distributed or state-dependent delays can be studied with the continuation software DDE-Biftool; for example, see Refs. 10 and 64. Figure 10 shows how the 1:2 resonance tongue of Fig. 7 changes under the influence of state-dependence as given by Eq. (7). As the value of $\eta$ is increased from $\eta = 0$ as in panel (a), there is a change in the parameter region where period-2 solutions exist. More specifically, there is symmetry-breaking within the family of period-2 solutions that results in curves SN of saddle-node bifurcations of (originally symmetrically related) periodic solution to no longer lie on top of each other; see panels (b) and (c) of Fig. 10. At the same time, the root point of the resonance tongue on curve T grows into a region of period-doubling. Also, notice that the overall region with locked dynamics increases considerably with $\eta$.

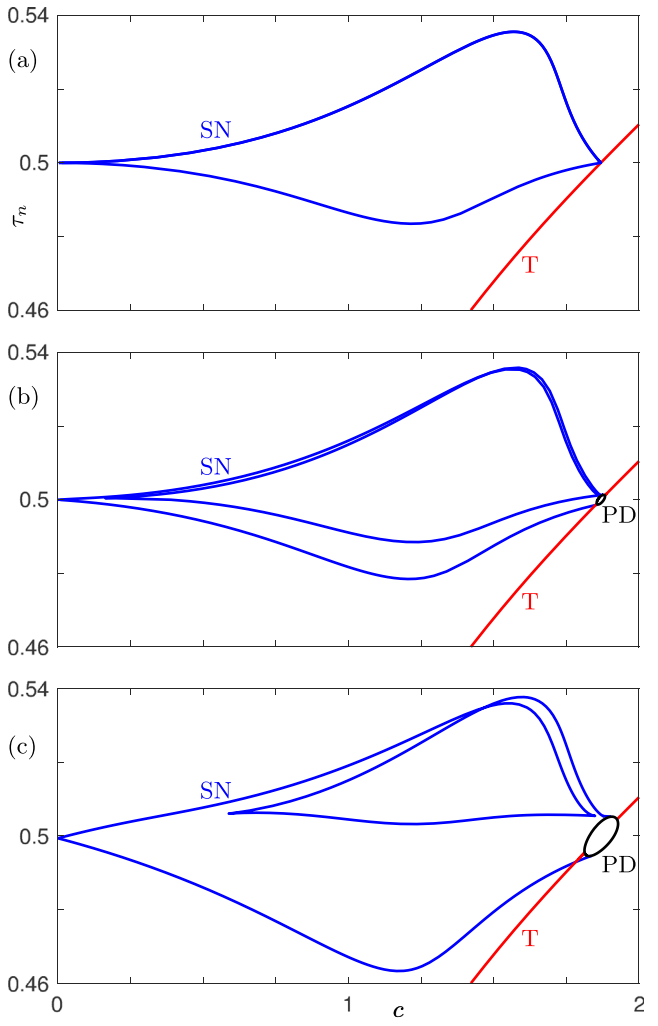


FIG. 10. Bifurcation set of Ghil-Zaliapin-Thompson model (5) in the $(c, \tau_n)$-plane with a state-dependent delay given by Eq. (7) with $\eta = 0$ (a), $\eta = 0.01$ (b) and $\eta = 0.04$ (c). Curves of torus (T) and period-doubling (PD) bifurcations are shown. Saddle-node bifurcations of periodic orbits (SN) form boundaries of a 1:2 resonance tongue. Other parameters are $b = 1$ and $\kappa = 11$.

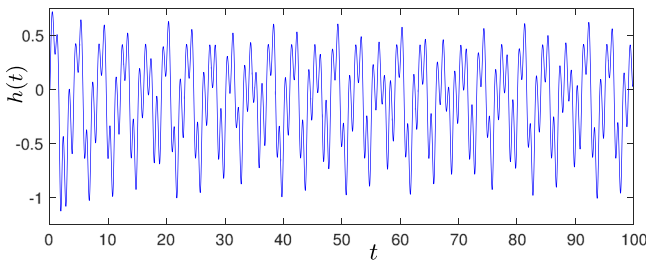


FIG. 11. Time series of model (4) with Eq. (7) for $\eta = 0.04$, calculated with Matlab's ddesd. Other parameters are $a = 2.02$, $b = 3.03$, $c = 2.6377$, $d_u = 2.0$, $d_l = -0.4$, $\tau_p = 0.0958$, $\tau_n = 0.4792$, and $\kappa = 1.5$.

Figure 11 shows a time series of model (4) with Eq. (7) for $\eta = 0.04$ to further demonstrate the effect of state-dependence; it was computed with the Matlab solver ddesd.[85] The time series shows irregular large temperature events and appears to be chaotic. This type of behaviour persists for about 2000 years, but then the trajectory finally settles into a complicated periodic solution with a very long period.

Equation (7) constitutes the simplest possible, yet realistic way to introduce state-dependence into an ENSO model. Despite this, and even though $\eta$ is small relative to $\tau_n$ in Figs. 10(c) and 11, our results show that state-dependence has the potential to play a significant role for generating realistic observable model behaviour. We believe that state-dependence in DDE climate models will emerge as an interesting direction for future research. Indeed, there are already a number of interesting questions: Is Eq. (7) an appropriate representation of state-dependent delay in a DAO model? Are there other important state-dependent effects and relationships? Would a distributed delay be more realistic and accurate? Should more focus be put on the resulting transient behaviour rather than eventual asymptotic behaviour?

## ACKNOWLEDGMENTS

We are grateful to an anonymous referee for helpful suggestions that led to an improved manuscript.

[1]L. S. Andersson and P. A. Lundberg, "Delayed albedo effects in a zero-dimensional climate model," J. Atmos. Sci. **45**, 2294–2305 (1988).
[2]K. Bar-Eli and R. J. Field, "Earth-average temperature: A time delay approach," J. Geophys. Res.: Atmos. **103**, 25949–25956, https://doi.org/10.1029/98JD02273 (1998).
[3]D. S. Battisti, "Dynamics and thermodynamics of a warming event in a coupled tropical atmosphere-ocean model," J. Atmos. Sci. **45**, 2889–2919 (1988).
[4]D. S. Battisti and A. C. Hirst, "Interannual variability in a tropical atmosphere-ocean model: Influence of the basic state, ocean geometry and nonlinearity," J. Atmos. Sci. **46**, 1687–1712 (1989).
[5]K. Bhattacharya, M. Ghil, and I. Vulis, "Internal variability of an energy-balance model with delayed albedo effects," J. Atmos. Sci. **39**, 1747–1773 (1982).
[6]M. F. Bierkens and B. J. Van den Hurk, "Groundwater convergence as a possible mechanism for multi-year persistence in rainfall," Geophys. Res. Lett. **34**, L02402, https://doi.org/10.1029/2006GL028396 (2007).
[7]K. Blaha, J. Lehnert, A. Keane, T. Dahms, P. Hövel, E. Schöll, and J. L. Hudson, "Clustering in delay-coupled smooth and relaxational chemical oscillators," Phys. Rev. E **88**, 062915 (2013).
[8]J.-P. Boulanger and C. Menkes, "Propagation and reflection of long equatorial waves in the Pacific Ocean during the 1992–1993 El Niño," J. Geophysical Res.: Oceans (1978–2012) **100**, 25041–25059 (1995).
[9]W. Buytaert, R. Célleri, and L. Timbe, "Predicting climate change impacts on water resources in the tropical Andes: Effects of GCM uncertainty," Geophys. Res. Lett. **36**, L07406, https://doi.org/10.1029/2008GL037048 (2009).
[10]R. C. Calleja, A. R. Humphries, and B. Krauskopf, "Resonance phenomena in a scalar delay differential equation with two state-dependent delays," SIAM J. Appl. Dyn. Syst. **16**(3), 1474 (2017).
[11]S. A. Campbell, "Time delays in neural systems," in *Handbook of Brain Connectivity* (Springer, 2007), pp. 65–90.
[12]M. A. Cane, M. Münnich, and S. F. Zebiak, "A study of self-excited oscillations of the tropical ocean-atmosphere system. Part I: Linear analysis," J. Atmos. Sci. **47**, 1562–1577 (1990).
[13]M. A. Cane, S. Zebiak, and S. Dolan, "Experimental forecasts of el nifio," Nature **321**, 827–832 (1986).
[14]M. A. Cane, S. E. Zebiak, and Y. Xue, "Model studies of the long-term behavior of ENSO," in *Natural Climate Variability on Decade-to-Century Time Scales* (The National Academies Press, Washington, DC, 1995), pp. 442–457.
[15]Y. Cao, "Uniqueness of periodic solution for differential delay equations," J. Differ. Equations **128**, 46–57 (1996).
[16]P. Chang, L. Ji, B. Wang, and T. Li, "Interactions between the seasonal cycle and El Niño-Southern oscillation in an intermediate coupled ocean-atmosphere model," J. Atmos. Sci. **52**, 2353–2372 (1995).
[17]S.-N. Chow and H.-O. Walther, "Characteristic multipliers and stability of symmetric periodic solutions of $\dot{x}(t) = g(x(t-1))$," Trans. Am. Math. Soc. **307**, 127–142 (1988).
[18]A. J. Clarke, J. Wang, and S. Van Gorder, "A simple warm-pool displacement ENSO model," J. Phys. Oceanogr. **30**, 1679–1691 (2000).
[19]M. Crucifix, "Oscillators and relaxation phenomena in Pleistocene climate theory," Philos. Trans. R. Soc. A **370**, 1140–1165 (2012).
[20]M. Darby and L. Mysak, "A Boolean delay equation model of an interdecadal Arctic climate cycle," Clim. Dyn. **8**, 241–246 (1993).
[21]S. De Gregorio, R. Pielke, and G. Dalu, "A delayed biophysical system for the Earth's climate," J. Nonlinear Sci. **2**, 293–318 (1992).
[22]H. De Jong, "Modeling and simulation of genetic regulatory systems: A literature review," J. Comput. Biol. **9**, 67–103 (2002).
[23]J. Díaz, A. Hidalgo, and L. Tello, "Multiple solutions and numerical analysis to the dynamic and stationary models coupling a delayed energy balance model involving latent heat and discontinuous albedo with a deep ocean," Proc. R. Soc. A **470**(2170), 20140376 (2014).
[24]O. Diekmann, S. A. Van Gils, S. M. Lunel, and H.-O. Walther, *Delay Equations: Functional-, Complex-, and Nonlinear Analysis*, Vol. 110 (Springer Science & Business Media, 2012).
[25]H. A. Dijkstra, *Nonlinear Physical Oceanography: A Dynamical Systems Approach to the Large Scale Ocean Circulation and El Niño*, Vol. 28 (Springer Science & Business Media, 2005).
[26]H. A. Dijkstra, *Nonlinear Climate Dynamics* (Cambridge University Press, 2013).
[27]H. A. Dijkstra and J. D. Neelin, "On the attractors of an intermediate coupled ocean-atmosphere model," Dyn. Atmos. Oceans **22**, 19–48 (1995).
[28]R. D. Driver, *Ordinary and Delay Differential Equations* (Springer-Verlag/New York Inc., 1977).
[29]K. Engelborghs, T. Luzyanina, and D. Roose, "Numerical bifurcation analysis of delay differential equations using DDE-BIFTOOL," ACM Trans. Math. Softw. **28**(1), 1–21 (2002).
[30]B. Ermentrout, *Simulating, Analyzing, and Animating Dynamical Systems: A Guide to XPPAUT for Researchers and Students* (SIAM, 2002).
[31]J. D. Farmer, "Chaotic attractors of an infinite-dimensional dynamical system," Phys. D: Nonlinear Phenom. **4**, 366–393 (1982).
[32]E. Galanti and E. Tziperman, "ENSO's phase locking to the seasonal cycle in the fast-SST, fast-wave, and mixed-mode regimes," J. Atmos. Sci. **57**, 2936–2950 (2000).
[33]M. Ghil, "Climate stability for a Sellers-type model," J. Atmos. Sci. **33**, 3–20 (1976).
[34]M. Ghil and K. Bhattacharya, "An energy-balance model of glaciation cycles," in *Report of the JOC Study Conference on Climate Models: Performance, Intercomparison and Sensitivity Studies*, edited by W. L. Gates (GARP Publ. Series No. 22, WMO/ICSU, Geneva, 1979), pp. 886–916.
[35]M. Ghil, A. Mullhaupt, and P. Pestiaux, "Deep water formation and Quaternary glaciations," Clim. Dyn. **2**, 1–10 (1987).
[36]M. Ghil, I. Zaliapin, and S. Thompson, "A delay differential model of ENSO variability: Parametric instability and the distribution of extremes," Nonlinear Processes Geophys. **15**, 417–433 (2008).

[37]N. E. Graham and W. B. White, "The El Niño cycle: A natural oscillator of the Pacific ocean-atmosphere system," Science **240**, 1293–1302 (1988).
[38]D. Gu and S. G. Philander, "Interdecadal climate fluctuations that depend on exchanges between the tropics and extratropics," Science **275**, 805–807 (1997).
[39]N. Guglielmi and E. Hairer, "Implementing Radau IIA methods for stiff delay differential equations," Computing **67**, 1–12 (2001).
[40]J. K. Hale and S. M. V. Lunel, *Introduction to Functional Differential Equations* (Springer-Verlag/New York Inc., 1993).
[41]G. Hetzer, "A functional reaction-diffusion equation from climate modeling: S-shapedness of the principal branch of fixed points of the time-1-map," Differ. Integr. Equations **8**(5), 1047–1059 (1995); available at https://projecteuclid.org:443/euclid.die/1369056043.
[42]G. Hetzer, "Global existence, uniqueness, and continuous dependence for a reaction-diffusion equation with memory," Electron. J. Differ. Equations **1996**, 1–16 (1996); available at http://eudml.org/doc/118886.
[43]G. Hetzer, "A quasilinear functional reaction-diffusion equation from climate modeling," Nonlinear Anal.: Theory, Methods Appl. **30**, 2547–2556 (1997).
[44]G. Hetzer, "S-shapedness for energy balance climate models of sellers-type," in *The Mathematics of Models for Climatology and Environment* (Springer, 1997), pp. 253–287.
[45]F.-F. Jin, "An equatorial ocean recharge paradigm for ENSO. Part I: Conceptual model," J. Atmos. Sci. **54**, 811–829 (1997).
[46]F.-F. Jin, "An equatorial ocean recharge paradigm for ENSO. Part II: A stripped-down coupled model," J. Atmos. Sci. **54**, 830–847 (1997).
[47]F.-F. Jin and J. D. Neelin, "Modes of interannual tropical ocean–atmosphere interaction-a unified view. part i: Numerical results," J. Atmos. Sci. **50**, 3477–3503 (1993).
[48]F.-F. Jin and J. D. Neelin, "Modes of interannual tropical ocean-atmosphere interaction: A unified view. Part III: Analytical results in fully coupled cases," J. Atmos. Sci. **50**, 3523–3540 (1993).
[49]F.-F. Jin, J. D. Neelin, and M. Ghil, "El Niño on the devil's staircase: Annual subharmonic steps to chaos," Science **264**, 70–72 (1994).
[50]E. Källén, C. Crafoord, and M. Ghil, "Free oscillations in a climate model with ice-sheet dynamics," J. Atmos. Sci. **36**, 2292–2303 (1979).
[51]H. Kaper and H. Engler, *Mathematics and Climate* (SIAM, 2013).
[52]A. Keane and B. Krauskopf, "Chenciner bubbles and torus break-up in a delay differential equation model for the El Niño Southern oscillation," preprint arXiv:1708.02334 (2017).
[53]A. Keane, B. Krauskopf, and C. Postlethwaite, "Delayed feedback versus seasonal forcing: Resonance phenomena in an El Niño Southern oscillation model," SIAM J. Appl. Dyn. Syst. **14**, 1229–1257 (2015).
[54]A. Keane, B. Krauskopf, and C. Postlethwaite, "Investigating irregular behavior in a model for the El Ninõ Southern oscillation with positive and negative delayed feedback," SIAM J. Appl. Dyn. Syst. **15**, 1656–1689 (2016).
[55]Y. S. Kolesov and D. Shvitra, "Role of time-delay in mathematical models of ecology," Lith. Math. J. **19**, 81–91 (1979).
[56]B. Krauskopf, "Bifurcation analysis of lasers with delay," *Unlocking Dynamical Diversity: Optical Feedback Effects Semiconductor Lasers* (John Wiley & Sons, Ltd., 2005), pp. 147–183.
[57]B. Krauskopf and K. Green, "Computing unstable manifolds of periodic orbits in delay differential equations," J. Comput. Phys. **186**, 230–249 (2003).
[58]B. Krauskopf and J. Sieber, "Bifurcation analysis of delay-induced resonances of the El-Niño Southern Oscillation," Proc. R. Soc. A **470**, 20140348 (2014).
[59]C. Kuehn, *Multiple Time Scale Dynamics*, Vol. 191 (Springer, 2015).
[60]Y. Kyrychko and S. Hogan, "On the use of delay equations in engineering applications," J. Vib. Control **16**, 943–960 (2010).
[61]Y. N. Kyrychko and K. B. Blyuss, "Global properties of a delayed sir model with temporary immunity and nonlinear incidence rate," Nonlinear Anal.: Real World Appl. **6**, 495–507 (2005).
[62]D. Lenstra, M. Yousefi, B. Krauskopf, and D. Lenstra, "Theory of delayed optical feedback in lasers," in *AIP Conference Proceedings* (AIP, 2000), Vol. 548, pp. 87–111.
[63]M. Lian and R. Cess, "Energy balance climate models: A reappraisal of ice-albedo feedback," J. Atmos. Sci. **34**, 1058–1062 (1977).
[64]T. Luzyanina and D. Roose, "Equations with distributed delays: Bifurcation analysis using computational tools for discrete delay equations," Funct. Differ. Equations **11**, 87 (2004).
[65]M. Münnich, M. A. Cane, and S. E. Zebiak, "A study of self-excited oscillations of the tropical ocean-atmosphere system. Part II: Nonlinear cases," J. Atmos. Sci. **48**, 1238–1248 (1991).
[66]J. D. Neelin, "The slow sea surface temperature mode and the fast-wave limit: Analytic theory for tropical interannual oscillations and experiments in a hybrid coupled model," J. Atmos. Sci. **48**, 584–606 (1991).
[67]J. D. Neelin and F.-F. Jin, "Modes of interannual tropical ocean–atmosphere interaction-a unified view. part ii: Analytical results in the weak-coupling limit," J. Atmos. Sci. **50**, 3504–3522 (1993).
[68]R. D. Nussbaum, "Uniqueness and nonuniqueness for periodic solutions of $x'(t) = -g(x(t-1))$," J. Differ. Equations **34**, 25–54 (1979).
[69]K. Parmar, K. B. Blyuss, Y. N. Kyrychko, and S. J. Hogan, "Time-delayed models of gene regulatory networks," Comput. Math. Methods Med. **2015**, 347273 (2015).
[70]C. Penland and P. D. Sardeshmukh, "The optimal growth of tropical sea surface temperature anomalies," J. Clim. **8**, 1999–2024 (1995).
[71]J. Picaut, F. Masia, and Y. Du Penhoat, "An advective-reflective conceptual model for the oscillatory nature of the ENSO," Science **277**, 663–666 (1997).
[72]Y. Pomeau and P. Manneville, "Intermittent transition to turbulence in dissipative dynamical systems," Commun. Math. Phys. **74**, 189–197 (1980).
[73]K. Pyragas, "Continuous control of chaos by self-controlling feedback," Phys. Lett. A **170**, 421–428 (1992).
[74]D. A. Randall, *General Circulation Model Development: Past, Present, and Future*, Vol. 70 (Academic Press, 2000).
[75]J. A. Rial, "Abrupt climate change: Chaos and order at orbital and millennial scales," Global Planet. Change **41**, 95–109 (2004).
[76]J. A. Rial and C. Anaclerio, "Understanding nonlinear responses of the climate system to orbital forcing," Quat. Sci. Rev. **19**, 1709–1722 (2000).
[77]D. Roose and R. Szalai, "Continuation and bifurcation analysis of delay differential equations," in *Numerical Continuation Methods for Dynamical Systems*, edited by B. Krauskopf and H. M. Osinga (Springer, 2007), pp. 359–399.
[78]E. S. Sarachik and M. A. Cane, *The El Niño-Southern Oscillation Phenomenon* (Cambridge University Press, 2010).
[79]A. Saunders and M. Ghil, "A Boolean delay equation model of ENSO variability," Phys. D: Nonlinear Phenom. **160**, 54–78 (2001).
[80]J. Saynisch, J. Kurths, and D. Maraun, "A conceptual ENSO model under realistic noise forcing," Nonlinear Processes Geophys. **13**, 275–285 (2006).
[81]C.-F. Schleussner, K. Frieler, M. Meinshausen, J. Yin, and A. Levermann, "Emulating Atlantic overturning strength for low emission scenarios: Consequences for sea-level rise along the North American east coast," Earth Syst. Dyn. **2**, 191–200 (2011).
[82]E. K. Schneider, B. Huang, and J. Shukla, "Ocean wave dynamics and El Niño," J. Clim. **8**, 2415–2439 (1995).
[83]E. Schöll, G. Hiller, P. Hövel, and M. A. Dahlem, "Time-delayed feedback in neurosystems," Philos. Trans. R. Soc. London A: Math. Phys. Eng. Sci. **367**, 1079–1096 (2009).
[84]W. D. Sellers, "A global climatic model based on the energy balance of the earth-atmosphere system," J. Appl. Meteorol. **8**, 392–400 (1969).
[85]L. Shampine, "Solving ODEs and DDEs with residual control," Appl. Numer. Math. **52**, 113–127 (2005).
[86]L. F. Shampine and S. Thompson, "Solving DDEs in Matlab," Appl. Numer. Math. **37**, 441–458 (2001).
[87]J. Sieber, K. Engelborghs, T. Luzyanina, G. Samaey, and D. Roose, "DDE-BIFTOOL manual—Bifurcation analysis of delay differential equations," preprint arXiv:1406.7144 (2014).
[88]J. Sieber, P. Kowalczyk, S. Hogan, and M. Di Bernardo, "Dynamics of symmetric dynamical systems with delayed switching," J. Vib. Control **16**, 1111–1140 (2010).
[89]H. Smith, *An Introduction to Delay Differential Equations with Applications to the Life Sciences*, Vol. 57 (Springer Science & Business Media, 2010).
[90]G. Stépán, *Retarded Dynamical Systems: Stability and Characteristic Functions* (Longman Scientific & Technical, 1989).
[91]L. Stone, P. I. Saparin, A. Huppert, and C. Price, "El Niño chaos: The role of noise and stochastic resonance on the ENSO cycle," Geophys. Res. Lett. **25**, 175–178, https://doi.org/10.1029/97GL53639 (1998).
[92]M. J. Suarez and P. S. Schopf, "A delayed action oscillator for ENSO," J. Atmos. Sci. **45**, 3283–3287 (1988).
[93]R. Szalai, G. Stépán, and S. John Hogan, "Continuation of bifurcations in periodic delay-differential equations using characteristic matrices," SIAM J. Sci. Comput. **28**, 1301–1317 (2006).
[94]C. Thompson and D. Battisti, "A linear stochastic dynamical model of ENSO. Part II: Analysis," J. Clim. **14**, 445–466 (2001).
[95]S. Thompson and L. Shampine, "A friendly Fortran DDE solver," Appl. Numer. Math. **56**, 503–516 (2006).

[96]Y. M. Tourre, B. Rajagopalan, Y. Kushnir, M. Barlow, and W. B. White, "Patterns of coherent decadal and interdecadal climate signals in the pacific basin during the 20th century," Geophys. Res. Lett. **28**, 2069–2072, https://doi.org/10.1029/2000GL012780 (2001).
[97]E. Tziperman, M. A. Cane, and S. E. Zebiak, "Irregularity and locking to the seasonal cycle in an ENSO prediction model as explained by the quasi-periodicity route to chaos," J. Atmos. Sci. **52**, 293–306 (1995).
[98]E. Tziperman, M. A. Cane, S. E. Zebiak, Y. Xue, and B. Blumenthal, "Locking of El Niño's peak time to the end of the calendar year in the delayed oscillator picture of ENSO," J. Clim. **11**, 2191–2199 (1998).
[99]E. Tziperman, L. Stone, M. A. Cane, and H. Jarosh, "El Niño chaos: Overlapping of resonances between the seasonal cycle and the Pacific ocean-atmosphere oscillator," Science **264**, 72–73 (1994).
[100]G. K. Vallis, *Climate and the Oceans* (Princeton University Press, 2012).
[101]C. Wang, "A unified oscillator model for the El Niño-Southern oscillation," J. Clim. **14**, 98–115 (2001).
[102]C. Wang and J. Picaut, "Understanding ENSO physics - A review," in *Earth's Climate: The Ocean-Atmosphere Interaction, Geophysical Monograph Series*, edited by C. Wang, S.-P. Xie, and J. A. Carton (AGU, Washington, D.C., 2004), Vol. 147, pp. 21–48.
[103]C. Wang, R. H. Weisberg, and J. I. Virmani, "Western Pacific interannual variability associated with the El Niño-Southern oscillation," J. Geophys. Res.: Oceans **104**, 5131–5149, https://doi.org/10.1029/1998JC900090 (1999).
[104]C. Wang, R. H. Weisberg, and H. Yang, "Effects of the wind speed-evaporation-SST feedback on the El Niño-Southern oscillation," J. Atmos. Sci. **56**, 1391–1403 (1999).
[105]R. H. Weisberg and C. Wang, "A western Pacific oscillator paradigm for the El Niño-Southern oscillation," Geophys. Res. Lett. **24**, 779–782, https://doi.org/10.1029/97GL00689 (1997).
[106]W. B. White and Y. M. Tourre, "A delayed action oscillator shared by the ENSO and QDO in the Indian Ocean," J. Oceanogr. **63**, 223–241 (2007).
[107]W. B. White, Y. M. Tourre, M. Barlow, and M. Dettinger, "A delayed action oscillator shared by biennial, interannual, and decadal signals in the Pacific Basin," J. Geophys. Res.: Oceans **108**, 3070 (2003).
[108]T. M. Wohlleben and A. J. Weaver, "Interdecadal climate variability in the subpolar North Atlantic," Clim. Dyn. **11**, 459–467 (1995).
[109]D. Wright, T. Stocker, and L. Mysak, "A note on quaternary climate modelling using boolean delay equations," Clim. Dyn. **4**, 263–267 (1990).
[110]I. Zaliapin and M. Ghil, "A delay differential model of ENSO variability—Part 2: Phase locking, multiple solutions and dynamics of extrema," Nonlinear Processes Geophys. **17**, 123–135 (2010).
[111]S. E. Zebiak and M. A. Cane, "A model El Niñ—Southern oscillation," Mon. Weather Rev. **115**, 2262–2278 (1987).
[112]H. Zelle, G. Appeldoorn, G. Burgers, and G. J. van Oldenborgh, "The relationship between sea surface temperature and thermocline depth in the eastern equatorial Pacific," J. Phys. Oceanogr. **34**, 643–655 (2004).
[113]K. Zickfeld, B. Knopf, V. Petoukhov, and H. Schellnhuber, "Is the Indian summer monsoon stable against global change?," Geophys. Res. Lett. **32**, https://doi.org/10.1029/2005GL022771 (2005).